Stanford Exploration Project, Report 105, September 5, 2000, pages 109–139

Tau tomography with steering filters: 3-D field data example, preliminary result

Robert G. Clapp[1]

ABSTRACT

I extend tau tomography into 3-D. I apply steering filter regularized tau tomography on a 3-D North Sea Dataset. Early results show promise.

INTRODUCTION

Velocity estimation, especially in 3-D, is one of the most important and difficult problems in exploration seismology. When the media is complex, a common solution is to linearize the non-linear tomography problem around an initial velocity estimate (van Trier, 1990; Etgen, 1990; Stork and Clayton, 1991). This linearization can potentially cause convergence problems. In previous papers (Clapp and Biondi, 1998, 1999a, 2000), I introduced a new way to approach this linearized inverse problem. Following the methodology introduced in Biondi et al. (1997), I reformulated the tomography operator from the depth domain to the tau domain. I showed how in the tau domain our linearized operator is less affected by velocity errors therefore we are back projecting velocity changes to more accurate locations (Clapp and Biondi, 1999b).

A major weakness of tomography is that it has a large null space and how we fill that null space has a major effect on both conversion speed and model quality. Velocity estimates derived from tomography tend to be *blobby* and not geologically plausible. To create more geologically reasonable velocity models, I regularize the tomography estimation problem with a steering filter (Clapp et al., 1997; Clapp, 2000). A steering filter is a space-varying operator composed of small plane-wave annihilators oriented along predefined dip directions derived from early migration results or other *a priori* information sources.

All these previous papers dealt with the 2-D velocity estimation problem. In this paper, I extend into 3-D the previously introduced concepts and apply my tomography method to a North Sea dataset provided by Elf Aquitaine. I begin by showing how the tau tomography operator can be formulated in 3-D. I then introduce the 3-D dataset and show residual moveout remaining in the common reflection point (CRP) gathers from the initial migration. Next I show how I built the 3-D steering filter operator for the dataset. I conclude by showing the results of applying my tomography methodology onto the dataset and comparing and contrasting

[1]**email:** bob@sep.stanford.edu

the migration results.

REVIEW

Following the methodology of Clapp and Biondi (1999a), I will begin by considering a regularized tomography problem. I will linearize around an initial slowness estimate and find a linear operator in the vertical traveltime domain $\mathbf{T}$ between our change in slowness $\Delta\mathbf{s}$ and our change in traveltimes $\Delta\mathbf{t}$. We will write a set of fitting goals,

$$\begin{aligned} \Delta\mathbf{t} &\approx \mathbf{T}\Delta\mathbf{s} \\ \mathbf{0} &\approx \epsilon\mathbf{A}\Delta\mathbf{s}, \end{aligned} \tag{1}$$

where $\mathbf{A}$ is our steering filter operator and ϵ is a Lagrange multiplier. However, these fitting goals don't accurately describe what we really want. Our steering filters are based on our desired slowness rather than change of slowness. With this fact in mind, we can rewrite our second fitting goal as:

$$\mathbf{0} \approx \epsilon\mathbf{A}(\mathbf{s_0}+\Delta\mathbf{s}) \tag{2}$$

$$-\epsilon\mathbf{A}\mathbf{s_0} \approx \epsilon\mathbf{A}\Delta\mathbf{s}. \tag{3}$$

Our second fitting goal can not be strictly defined as regularization but we can do a preconditioning substitution (Fomel et al., 1997), giving us a new set of fitting goals:

$$\begin{aligned} \Delta\mathbf{t} &\approx \mathbf{T}\mathbf{A}^{-1}\mathbf{p} \\ -\epsilon\mathbf{A}\mathbf{s_0} &\approx \epsilon\mathbf{I}\mathbf{p}. \end{aligned} \tag{4}$$

EXTENSION TO 3-D

To construct $\mathbf{T}$ we must derive a relationship between dt and $\Delta\mathbf{s}$. We will begin by defining two different slownesses: focusing and mapping slowness. The focusing slowness is the slowness that best focuses the data. The mapping slowness is the slowness that correctly positions the data.

Starting with mapping slowness s_m in terms of x,y, and z, we can transform into tau space through

$$\begin{aligned} \tau(z,x,y) &= \int_0^z 2s_m(z',x,y)dz' \\ x' &= x \\ y' &= y, \end{aligned} \tag{5}$$

where τ is the two-way vertical traveltime, x' is our new x coordinate, and y' is our new y coordinate. Using the chain rule we can derive the relationship between the derivatives of our

coordinates,

$$\frac{\partial t}{\partial z} = \frac{\partial t}{\partial \tau}\frac{\partial \tau}{\partial z}+\frac{\partial t}{\partial x'}\frac{\partial x'}{\partial z}+\frac{\partial t}{\partial y'}\frac{\partial y'}{\partial z}=\frac{\partial t}{\partial \tau}2s_m(z,x,y) \tag{6}$$

$$\frac{\partial t}{\partial x} = \frac{\partial t}{\partial \tau}\frac{\partial \tau}{\partial x}+\frac{\partial t}{\partial x'}\frac{\partial x'}{\partial x}+\frac{\partial t}{\partial y'}\frac{\partial y'}{\partial x}=\frac{\partial t}{\partial x'}+\frac{\partial t}{\partial y'}+\frac{\partial t}{\partial \tau}\int_0^z \frac{\partial}{\partial x}2s_m(z',x,y)dz' \tag{7}$$

$$\frac{\partial t}{\partial y} = \frac{\partial t}{\partial \tau}\frac{\partial \tau}{\partial y}+\frac{\partial \tau}{\partial x'}+\frac{\partial x'}{\partial y}+\frac{\partial t}{\partial y'}\frac{\partial y'}{\partial y}=\frac{\partial t}{\partial y'}+\frac{\partial t}{\partial \tau}\int_0^z \frac{\partial}{\partial y}2s_m(z',x,y)dz'. \tag{8}$$

We can simplify the above relations by defining two σ quantities, one in the x-direction, σ_x, and one in the y-direction, σ_y,

$$\sigma_x(z,x,y) = \int_0^z \frac{\partial}{\partial x}2s_m(z',x,y)dz' \tag{9}$$

$$\sigma_y(z,x,y) = \int_0^z \frac{\partial}{\partial y}2s_m(z',x,y)dz'. \tag{10}$$

Taking the derivative of both sides of the transform of (5) we can obtain a relation for dz, dx, and dy,

$$dz = \frac{d\tau}{2s_m}-\frac{\sigma_x dx'}{2s_m}-\frac{\sigma_y dy'}{2s_m} \tag{11}$$

$$dx = dx' \tag{12}$$

$$dy = dy'. \tag{13}$$

To obtain our tomography operator in 3-D we begin by defining the traveltime along a single ray segment (where quantities measured along the ray segment are indicated by $\widetilde{\ }$) in tau space using equations (11-13),

$$\widetilde{dt}=\sqrt{\left(\widetilde{S_f}\widetilde{dx'}\right)^2+\left(\widetilde{S_f}\widetilde{dy'}\right)^2+\left(\frac{\widetilde{d\tau}-\widetilde{\sigma_x}\widetilde{dx'}-\widetilde{\sigma_y}\widetilde{dy'}}{2}\right)^2} \tag{14}$$

We can then take the derivative with respect to the focusing slowness s_f,

$$\frac{d(\widetilde{dt})}{dS_f}=\frac{\widetilde{S_f}\left(\widetilde{dx'}^2+\widetilde{dy'}^2\right)}{\widetilde{dt}}\frac{d\widetilde{S_f}}{ds_f}-\frac{\left(\widetilde{d\tau}-\widetilde{dx'}\widetilde{\sigma_x}-\widetilde{dy'}\widetilde{\sigma_y}\right)}{4\widetilde{dt}}\left(\widetilde{dx'}\frac{d\widetilde{\sigma_x}}{ds_f}+\widetilde{dy'}\frac{d\widetilde{\sigma_y}}{ds_f}.\right) \tag{15}$$

We new have an expression in terms of $\frac{d\widetilde{S_f}}{ds_f}$, $\frac{d\widetilde{\sigma_x}}{ds_f}$, and $\frac{d\widetilde{\sigma_y}}{ds_f}$. To get an expression in terms of just $\frac{d\widetilde{S_f}}{ds_f}$ we start by taking the partial derivative of τ with respect to x',

$$\frac{\partial \tau}{\partial x'} = \frac{\partial \tau}{\partial x}\frac{\partial x}{\partial x'}+\frac{\partial \tau}{\partial y}\frac{\partial y}{\partial x'}+\frac{\partial \tau}{\partial z}\frac{\partial z}{\partial x'} \tag{16}$$

$$\frac{\partial \tau}{\partial x}\frac{\partial x}{\partial x'} = \frac{\partial}{\partial z}\int_0^z 2s(z',x,y)dz'$$

$$\sigma_x = -2s_f(\tau,x')\frac{\partial z}{\partial x}$$

$$\sigma_x(z,x,y) = -s_f(\tau,x',y)\int_0^\tau \frac{\partial}{\partial x'}\frac{1}{s_f(\tau',x',y')}d\tau'$$

and similarly

$$\sigma_y(z,x,y) = -s_f(\tau,x,y') \int_0^\tau \frac{\partial}{\partial y'} \frac{1}{s_f(\tau',x',y')} d\tau'. \tag{17}$$

We then take the derivative with respect to s_f and evaluate at the ray segment,

$$\frac{\partial \widetilde{\sigma_x}}{\partial s_f} = \frac{\widetilde{\sigma_x}}{\widetilde{S_f}} \frac{\partial \widetilde{S_f}}{\partial s_f} - \widetilde{S_f} \int_0^\tau \frac{\partial^2 s_f(\tau',x',y')}{\partial x' \partial s_f} \partial \tau' \tag{18}$$

$$\frac{\partial \widetilde{\sigma_y}}{\partial s_f} = \frac{\widetilde{\sigma_y}}{\widetilde{S_f}} \frac{\partial \widetilde{S_f}}{\partial s_f} - \widetilde{S_f} \int_0^\tau \frac{\partial^2 s_f(\tau',x',y')}{\partial y' \partial s_f} \partial \tau'. \tag{19}$$

As a result we now have a linear relation between $\Delta \mathbf{t}$ and S_f in the tau domain.

DATA

The data were acquired over a salt dome using three cables of 3570m length with geophones every 25m. The CMP sampling inline was 13.33m and crossline of 25m. The entire survey covered 13.5km inline and 4km crossline. Although this is not an exceptionally large 3-D survey, tomography is an iterative process so reducing the cost of the migration is an important consideration. For tomography, well implemented Kirchhoff methods which can produce a sparse set of CRP gathers are ideal. An alternate approach when dealing with marine data is Common Azimuth Migration (CAM) (Biondi and Palacharla, 1996). CAM requires more expensive full volume imaging, but provided three advantages to me:

- it is faster than Kirchoff when performing full volume imaging
- it can easily produce model domain angle gathers (Prucha et al., 1999; Sava and Fomel, 2000)
- it was already implemented in SEPlib

This dataset has been previously migrated using CAM (Vaillant and Sava, 1999; Vaillant and Calandra, 2000) at SEP. In this paper, and the previous papers, the data volume was reduced to 10.5km inline and 4km crossline. CAM operates in the frequency-wavenumber domain so the data had to be placed on a regular grid. Data regularization was performed using Azimuth Moveout (AMO) (Biondi et al., 1998). In the process of performing AMO the dataset was resampled. The resampled dataset had CMP spacing of 20m in the inline and 25m in the crossline. The offset range was resampled to 50m ranging from 200m to 3400m. This paper is simply attempt to prove that the concept works in 3-D, so for computational speed I decided to concentrate on the first 2500m in depth. Therefore I began by using only the first 3 seconds of the data. By windowing the data I was able to reduce the number of frequencies needed from 176 to 108 while still being able to handle frequencies up to 54Hz.

The initial velocity model was created using the S.M.A.R.T[2] method (Jacobs et al., 1992; Ehinger and Lailly, 1995). Early migration tests showed that a better migration result could be obtained by smoothing the model (Vaillant and Sava, 1999) . As a result the S.M.A.R.T. model was smoothed, preserving the sharp salt boundary (Figure 1). Using the velocity in Figure 1 the data was migrated with six reference velocities and frequency range of 5 to 60 Hz (Vaillant and Calandra, 2000). Figure 2 shows the initial migration result. Note how the reflectors generally have good coherency but die out at the top of the salt and along the salt flanks.

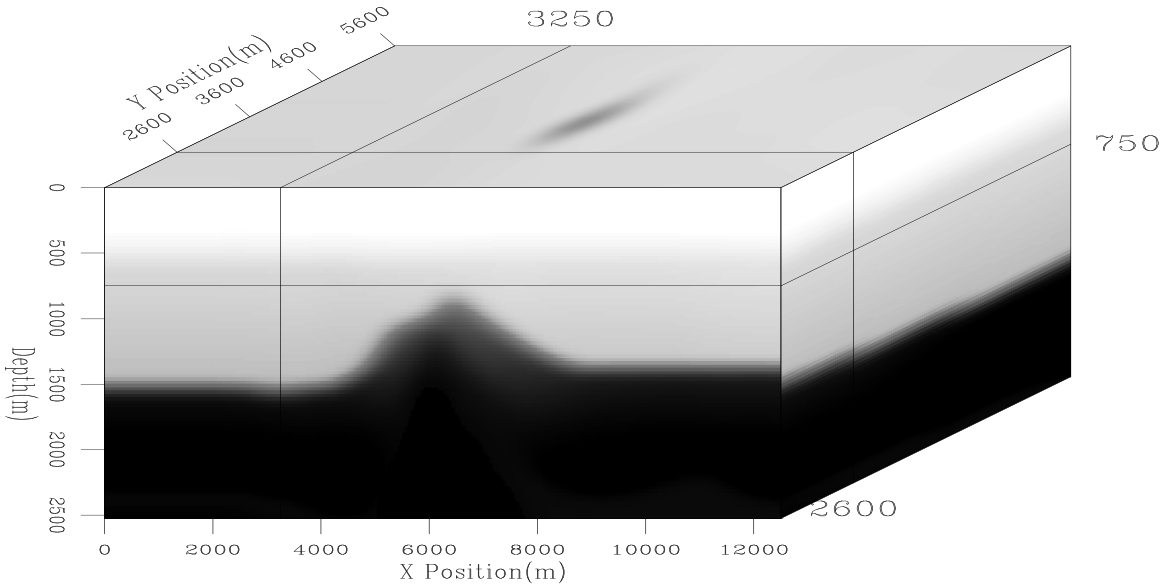

Figure 1: Initial ELF velocity model. bob1-elf3d.vel0 [ER]

INITIAL ERRORS

From the initial migration I chose five reflectors to perform tomography with (Figure 3). To constrain the upper portion of the model I chose the sea bottom reflection. 2-D tomography tests (Clapp and Biondi, 2000) indicated that largest error in the upper portion of the model was below the reflection at $1600m$. As a result I chose this reflector along with the salt top reflection and two reflectors on either side of the salt dome. To handle the steering filter dip calculation more accurately, I extend the reflectors on either side of salt artificially into the salt.

Excluding the artificially created reflector portions, I then calculated residual moveout along each of the reflectors (Figure 4). Generally the second reflector showed little to no moveout errors while the three below showed some moveout error, especially directly above and the edge of the salt body.

[2]Sequential Migration-Aided Reflection Tomography - KIM (Kinematic Inversion Methods), IFP consortium

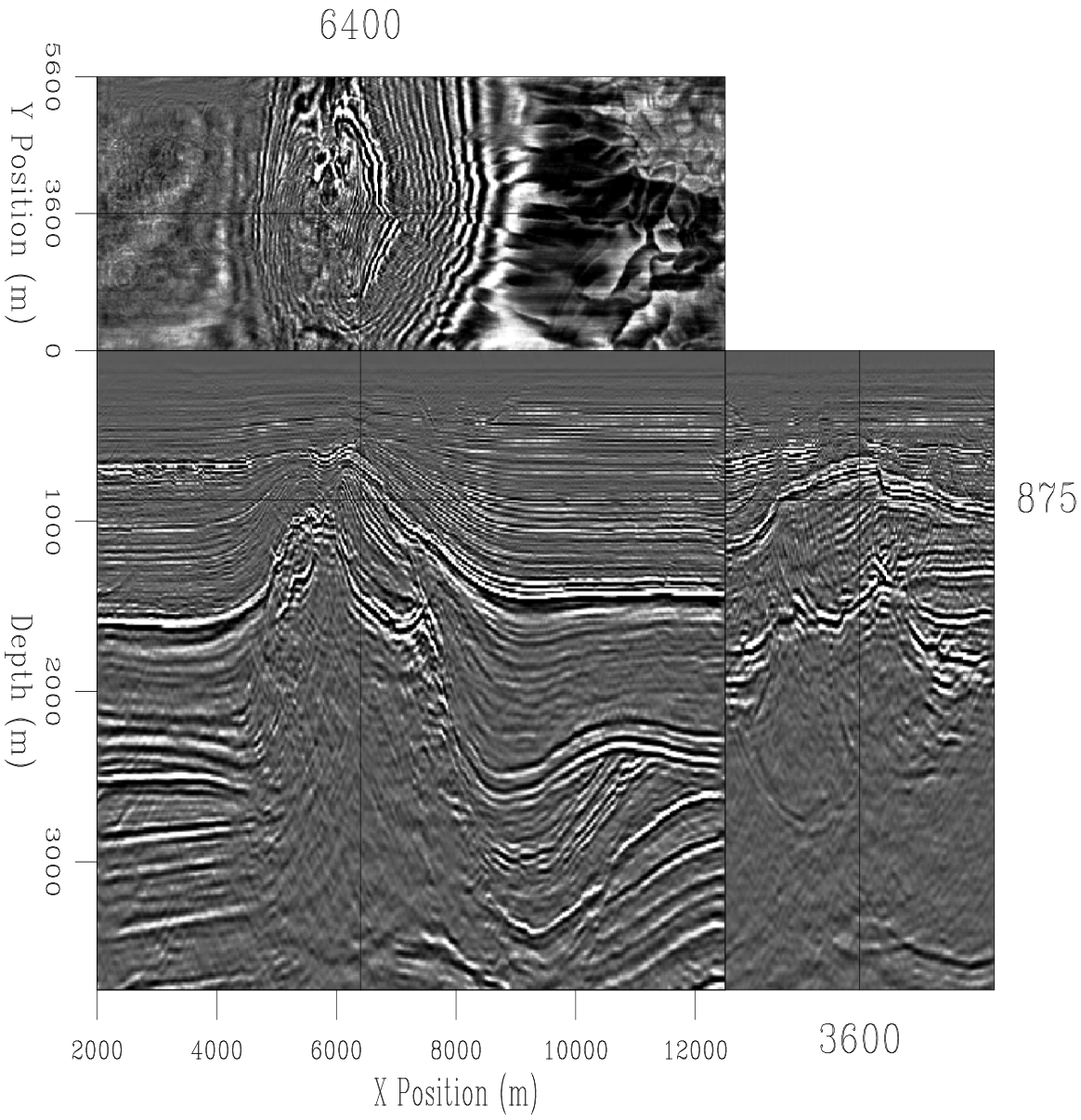

Figure 2: Initial migration using the velocity in Figure 1. bob1-elf3d.mig.vel0 [CR]

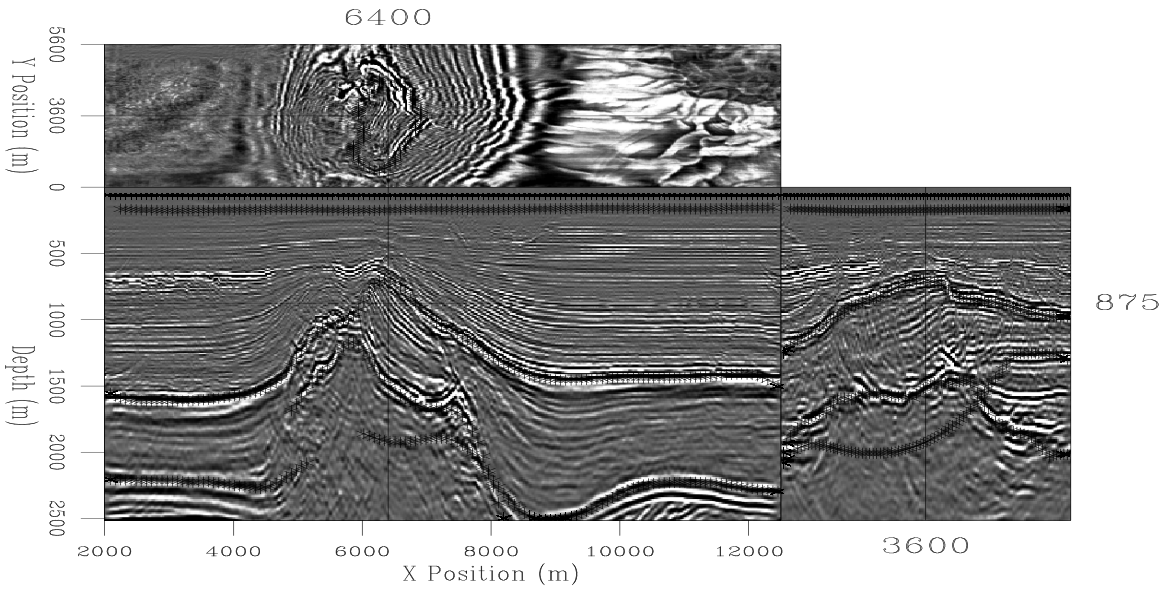

Figure 3: Five reflectors used in tomography superimposed on the initial migration image. Note how two of the reflectors were extended into the salt to create better smoothing directions for the steering filter. bob1-elf3d.reflectors.vel0 [CR]

Building the steering filters

To construct the 3-D steering filter operator I followed the methodology described in Clapp (2000), cascading two 2-D steering filter operators to form my 3-D steering filter operator. I used the five reflectors picked in the last section. To calculate the dip field I began by calculating the slope in the $x-z$ and $y-z$ planes. I mapped these two dip fields into (x,y,τ) model space. I then interpolated the field to the entire model space.

Once I had the dips in both the $x-z$ and $y-z$ planes I constructed two filter banks which encompassed the range of dips in each direction. It was then a simple matter of creating a mapping operator that mapped the dip at a given model point to a specific filter in the bank. To see the effect of this new complex operator I filled the model with random noise and then applied $A_{3d}\,A'_{3d}$ (Figure 5). As you can see the 3-D steering filter does a good job in spreading energy along reflector directions.

RESULTS

I applied the fitting goals (4) and obtained a $\Delta\mathbf{s}$ (Figure 6). The change introduced by tomography was a spatially low frequency increase in the velocity below the second tomography reflector. The decrease in slowness agreed with previous 2-D tomography tests (Clapp and Biondi, 2000). After adding in the slowness I ended up with an updated velocity field (Figure 7). The new velocity field is very consistent with the initial model (Figure 1).

Using the updated velocity field I applied CAM. Figure 9 shows the migration result.

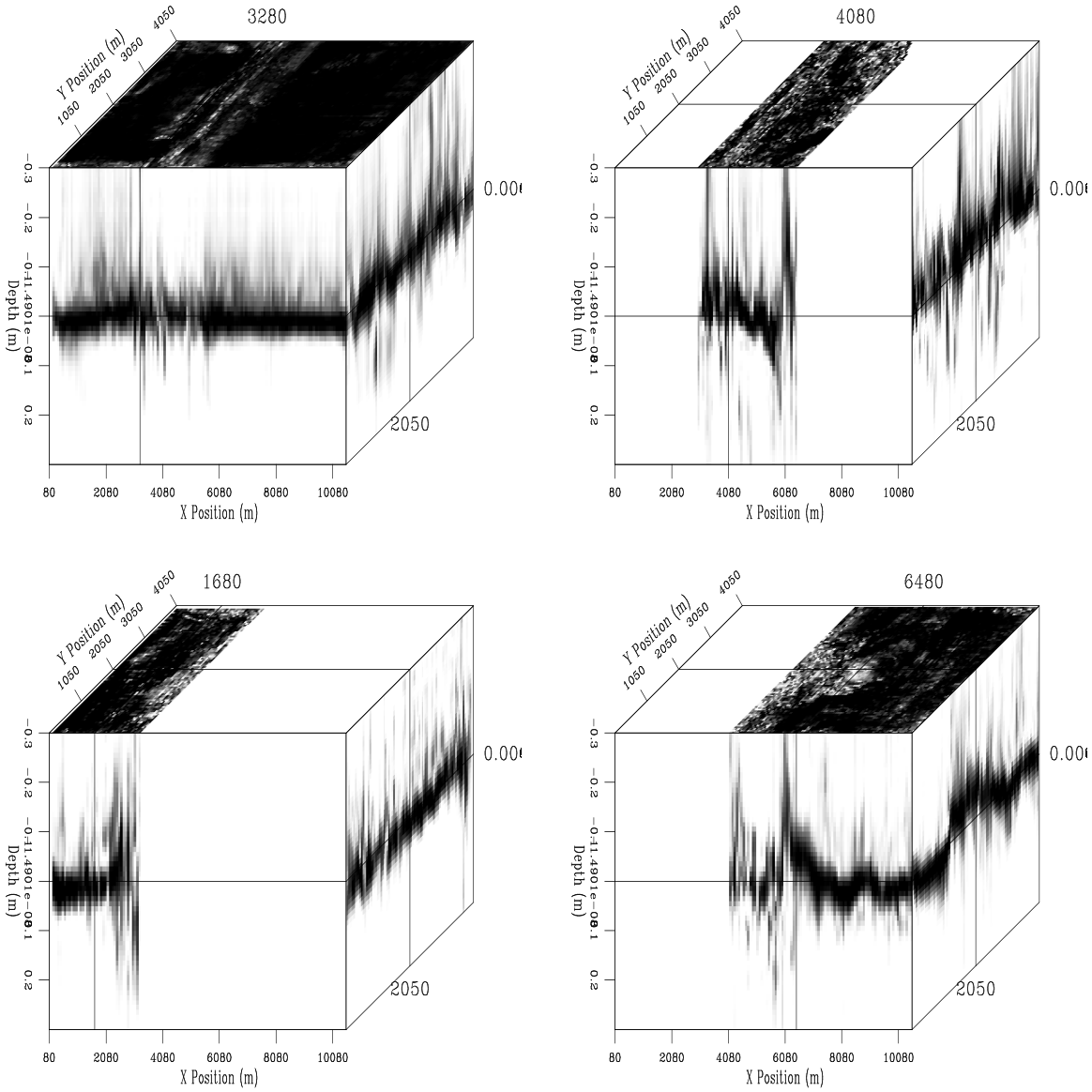

Figure 4: Initial semblance errors along the lower four reflectors used in tomography. bob1-elf3d.semb [CR]

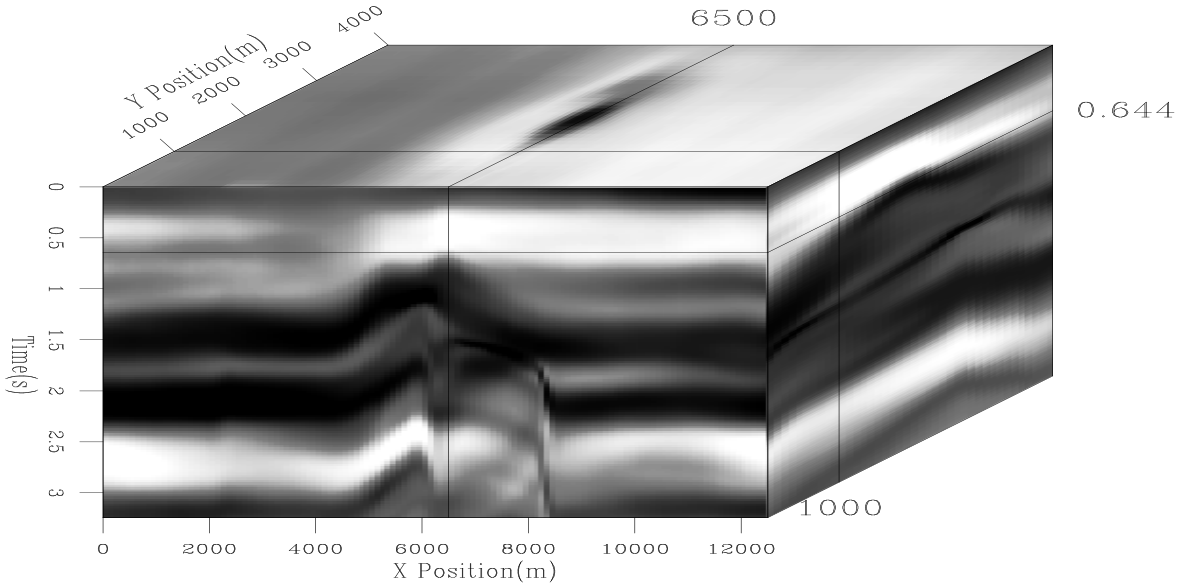

Figure 5: The result of putting random numbers into the model then applying $A_{3d}A'_{3d}$. bob1-random-3d [CR]

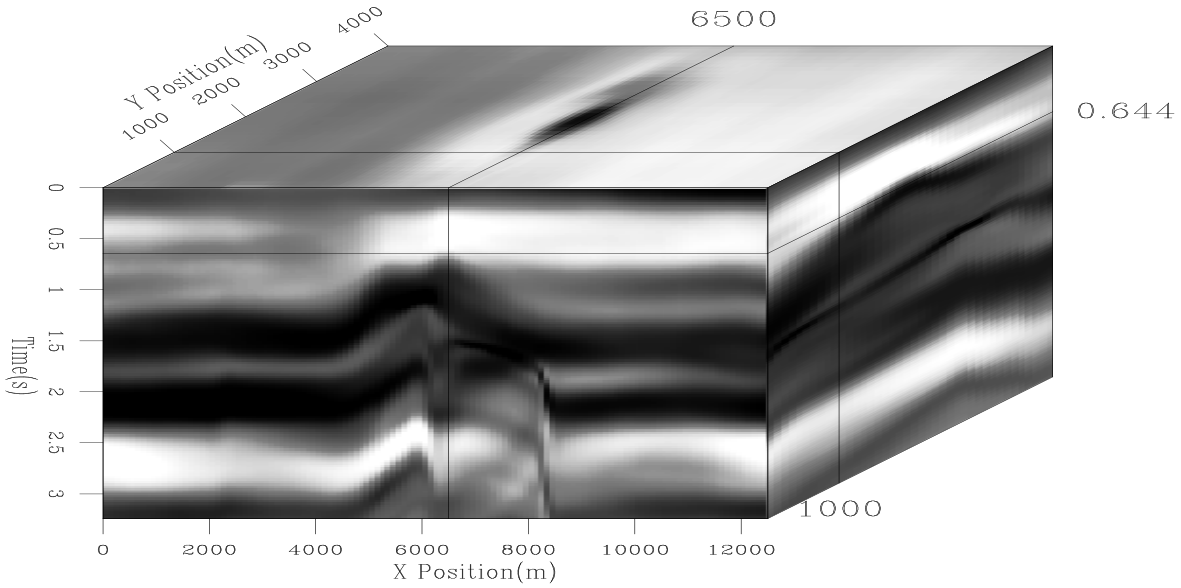

Figure 6: Changes to velocity computed from first iteration of tomography. bob1-ds-3d [CR]

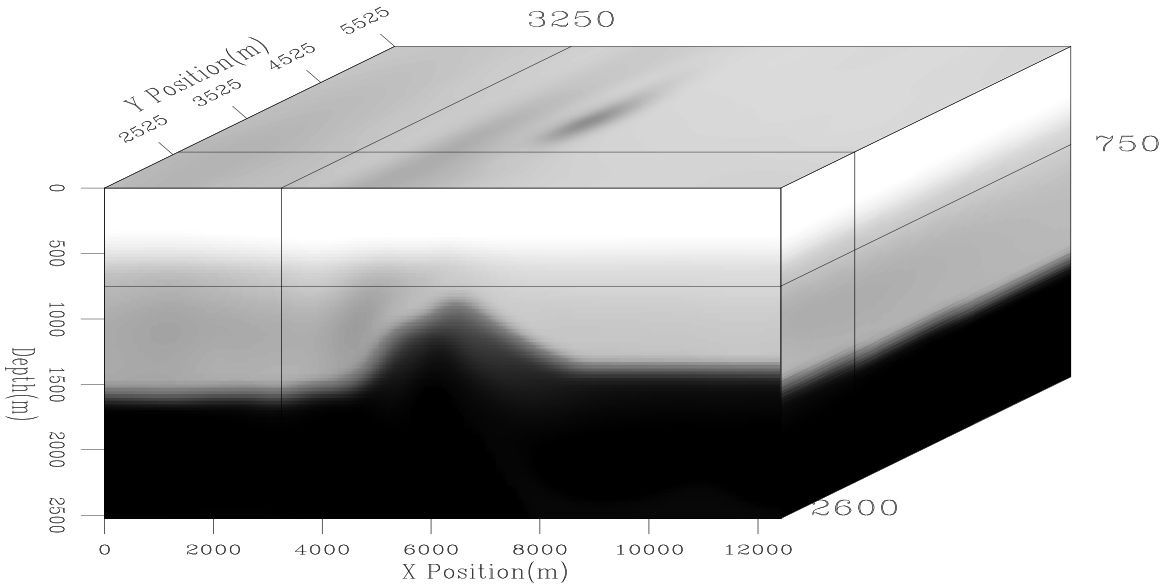

Figure 7: Velocity after one iteration of tomography. bob1-elf3d.vel1 [CR]

Generally, the image quality is about the same or slightly improved. Note that image is worse at ‘B’ (compared to the initial migration (Figure 8). At ‘A’ the initial image shows better coherence but the new migration has a higher frequency content. A sharper image can also be observed at ‘C’ - ‘F’. If we compare common reflection point gathers (Figure 10 and 11) we get a similar story. At ‘A’, ‘B’, and ‘E’ the gathers are flatter and higher frequency. At ‘C’ and ‘D’ where the gathers curved up initially they now curve down.

What next?

The unimpressive improvement in the image quality seems to be due to two factors. First, the introduced slowness change was too low in spatial frequency. The initial slowness model was already well determined for features at this scale. In addition, 2-D tests showed that image quality was most improved when allowing smaller scale changes to the velocity. Relaxing the smoothness constraint (by both decreasing ϵ in fitting goals (4) and iterating more) is called for. The second weakness seems to be poor constraint of the lower portion of the model. The obvious answer is to pick more reflectors. Both of these changes have been made, but unfortunately time constraints did not allow the results to be included in this paper.

CONCLUSIONS

Early results indicate that the tomography method is effective in 3-D. Overall image quality improvement is disappointing and relaxing of the smoothing constraint is warranted.

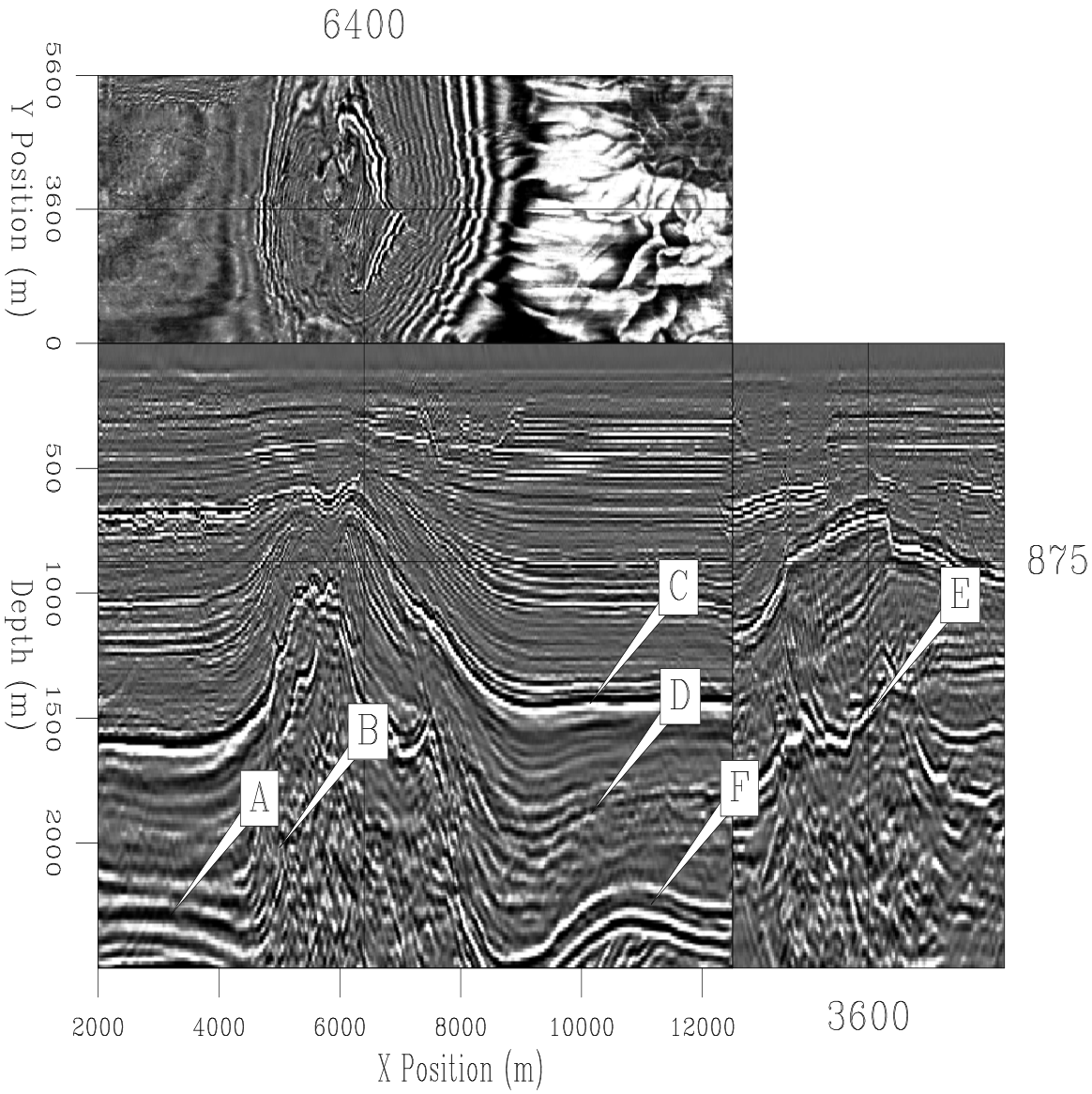

Figure 8: Migration result using initial velocity model. Overlaid are several locations where image quality changes with the new velocity model. bob1-elf3d.mig0.v2 [CR]

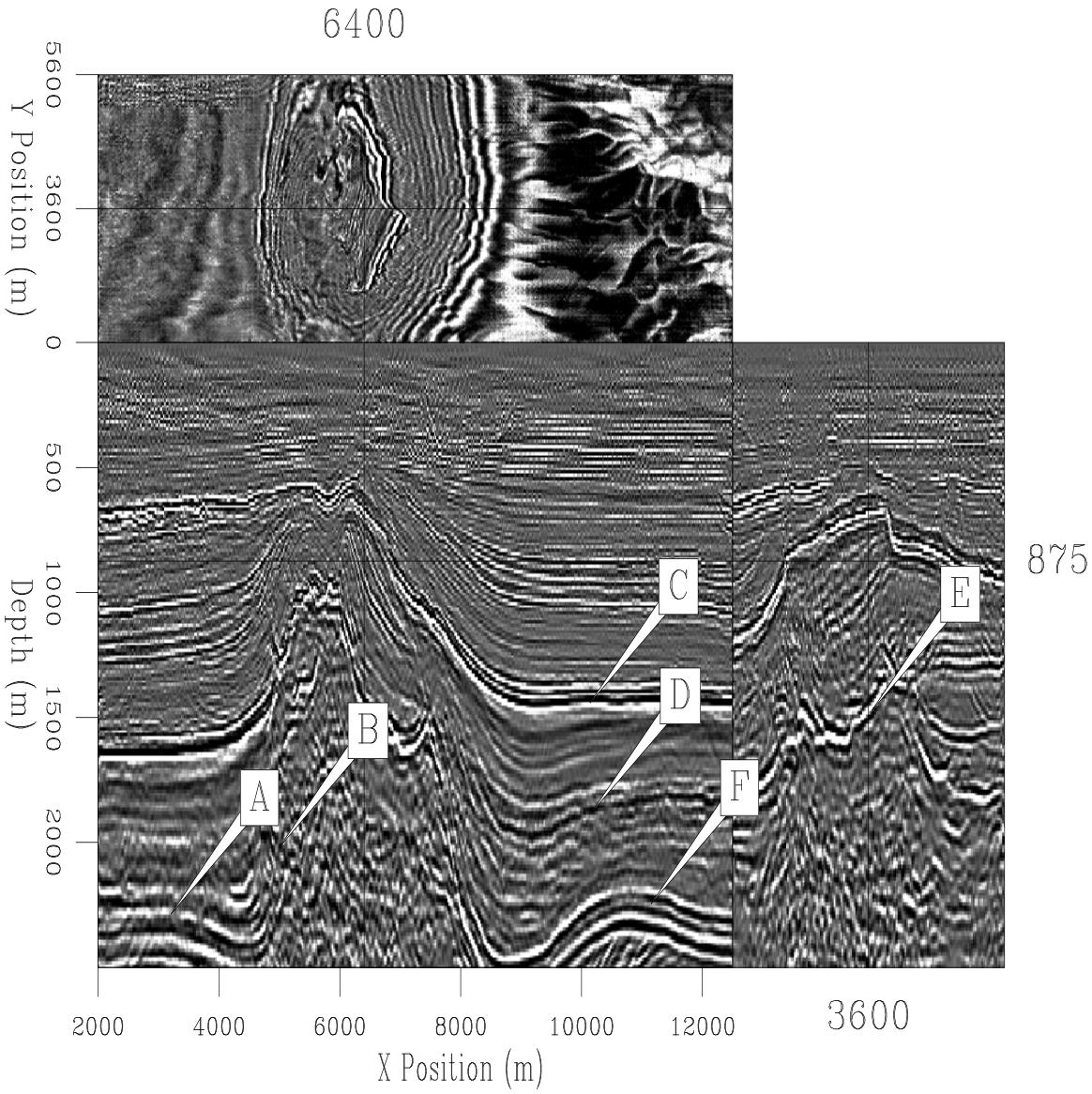

Figure 9: Migration result after one iteration of tomography. Note that image is worse at ‘B’ (compared to the initial migration (Figure 8). At ‘A’ the initial image show better coherence but the new migration is higher frequency content. A sharper image can also be observed at ‘C’ - ‘F’. bob1-elf3d.mig1.steer [CR,M]

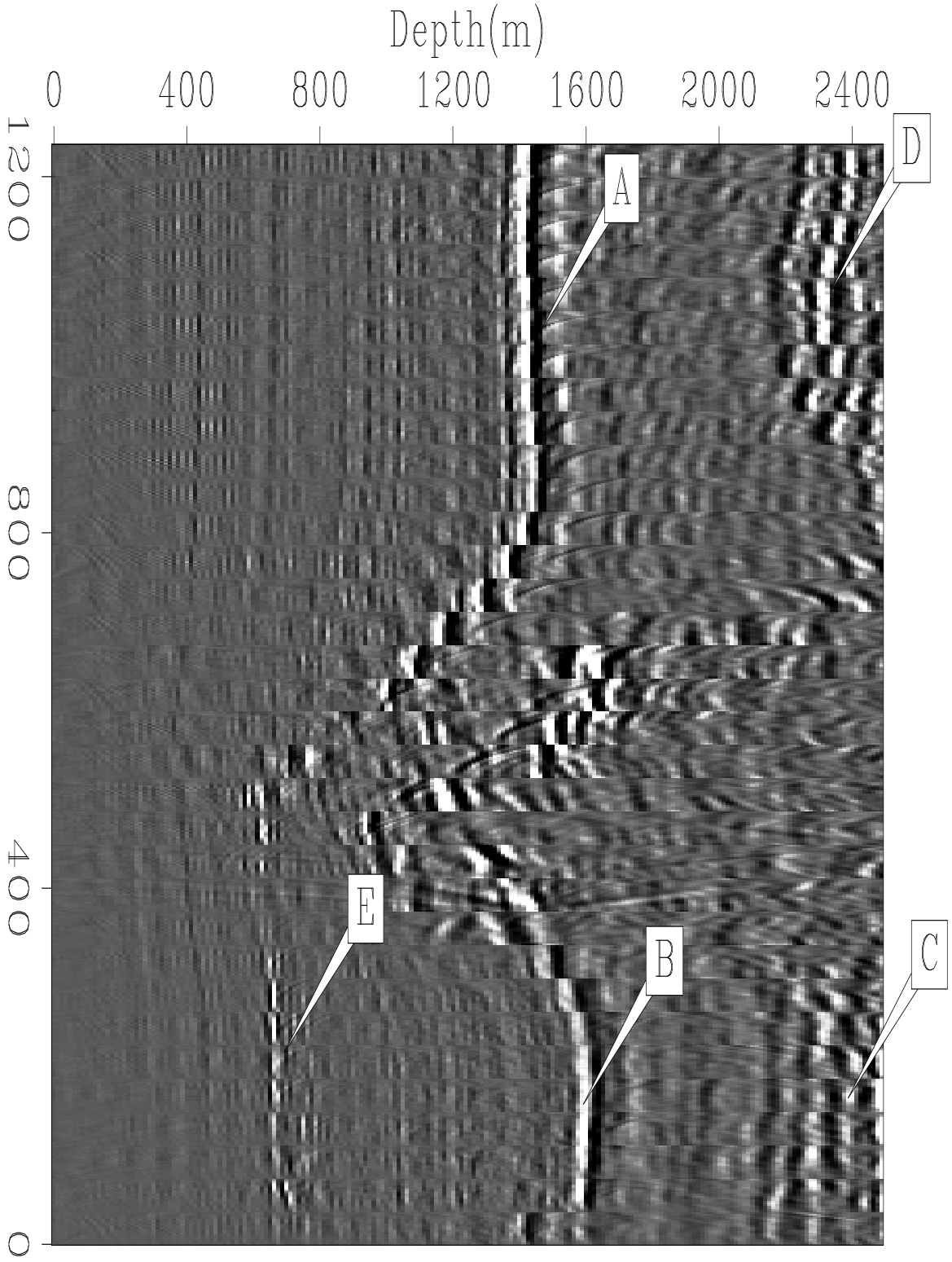

Figure 10: Every 20th CRP from an inline section of the initial migration. bob1-gather.vel0 [CR]

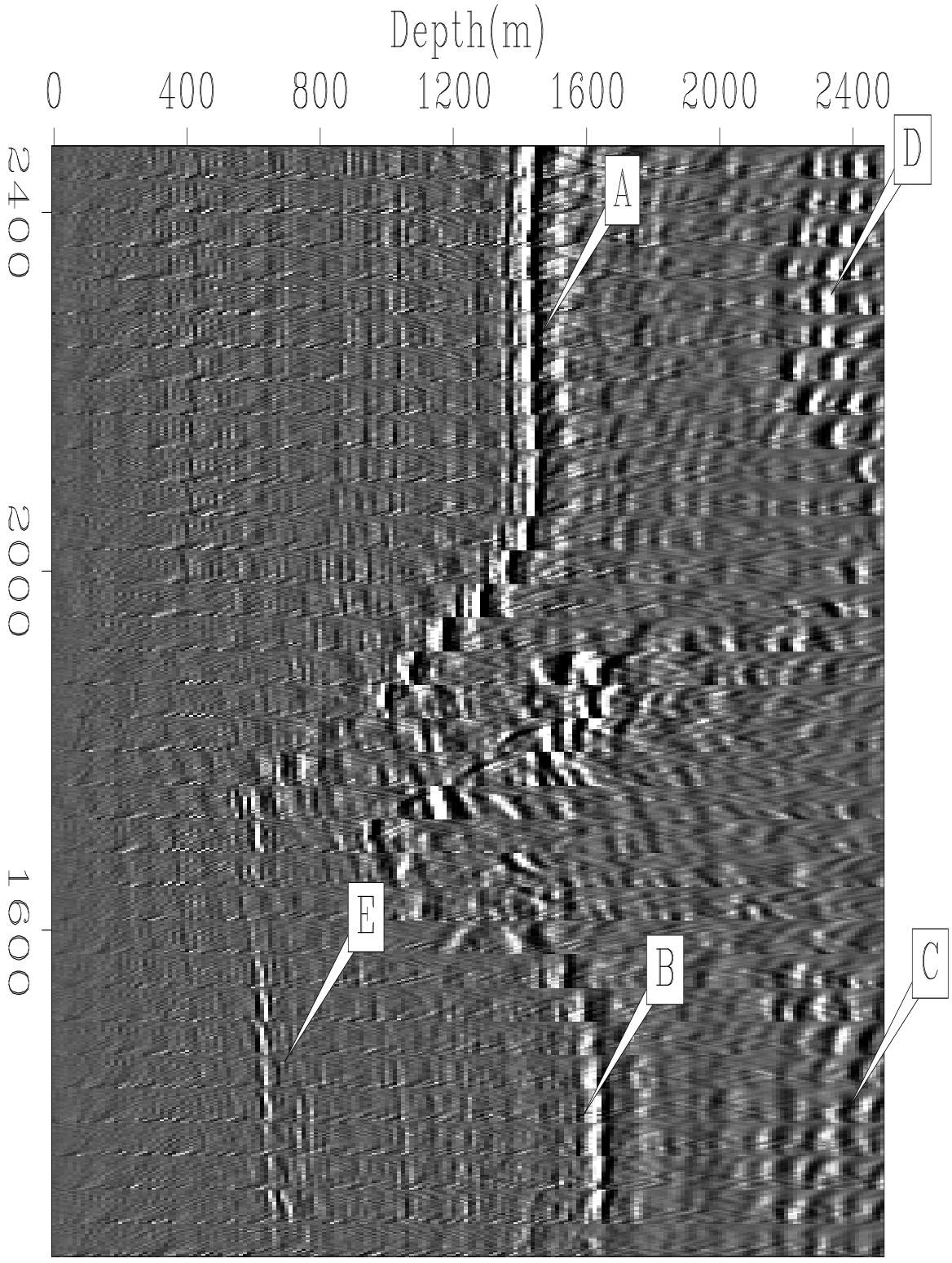

Figure 11: Every 20th CRP from an inline section of the migration after one iteration of tomography. At ‘A’, ‘B’, and ‘E’ the gathers are flatter and higher frequency than the gathers in Figure 10. At ‘C’ and ‘D’ where the gathers curved up initially they now curve down. bob1-gather.vel1.steer [CR,M]

ACKNOWLEDGMENTS

I would like to thank Elf for providing the data and Louis Vaillant for pre-processing the data and providing the initial migrated image.

REFERENCES

Biondi, B., and Palacharla, G., 1996, 3-D prestack migration of common-azimuth data: Geophysics, **61**, no. 6, 1822–1832.

Biondi, B., Fomel, S., and Alkhalifah, T., 1997, "Focusing" eikonal equation and global tomography: SEP–**95**, 61–76.

Biondi, B., Fomel, S., and Chemingui, N., 1998, Azimuth moveout for 3-D prestack imaging: Geophysics, **63**, no. 2, 574–588.

Clapp, R. G., and Biondi, B. L., 1998, Regularizing time tomography with steering filters: SEP–**97**, 137–146.

Clapp, R. G., and Biondi, B., 1999a, Preconditioning tau tomography with geologic constraints: SEP–**100**, 35–50.

Clapp, R. G., and Biondi, B., 1999b, Why tau tomography is better than depth tomography: SEP–**100**, 51–58.

Clapp, R. G., and Biondi, B. L., 2000, Tau tomography with steering filters: 2-D field data example: SEP–**103**, 1–19.

Clapp, R. G., Fomel, S., and Claerbout, J., 1997, Solution steering with space-variant filters: SEP–**95**, 27–42.

Clapp, R., 2000, 3-D steering filters: SEP–**105**, 109–116.

Ehinger, A., and Lailly, P., 1995, Velocity model determination by the SMART method, part 1: Theory: 65th Annual Internat. Mtg., Soc. Expl. Geophys., Expanded Abstracts, 739–742.

Etgen, J., 1990, Residual prestack migration and interval velocity estimation: Ph.D. thesis, Stanford University.

Fomel, S., Clapp, R., and Claerbout, J., 1997, Missing data interpolation by recursive filter preconditioning: SEP–**95**, 15–25.

Jacobs, J. A. C., Delprat-Jannaud, F., Ehinger, A., and Lailly, P., 1992, Sequential migration-aided reflection tomography: A tool for imaging complex structures: 62nd Annual Internat. Mtg., Soc. Expl. Geophys., Expanded Abstracts, 1054–1057.

Prucha, M. L., Biondi, B. L., and Symes, W. W., 1999, Angle-domain common image gathers by wave-equation migration: SEP–**100**, 101–112.

Sava, P., and Fomel, S., 2000, Angle-gathers by Fourier Transform: SEP–**103**, 119–130.

Stork, C., and Clayton, R. W., 1991, An implementation of tomographic velocity analysis: Geophysics, **56**, no. 04, 483–495.

Vaillant, L., and Calandra, H., 2000, Common-azimuth migration and Kirchhoff migration for 3-D prestack imaging: A comparison on North Sea data: SEP–**103**, 139–147.

Vaillant, L., and Sava, P., 1999, Common-azimuth migration of a North Sea dataset: SEP–**102**, 1–14.

van Trier, J., 1990, Tomographic determination of structural velocities from depth migrated seismic data: Ph.D. thesis, Stanford University.